

Classification of Segments in PolSAR Imagery by Minimum Stochastic Distances Between Wishart Distributions

Wagner B. Silva, Corina C. Freitas, Sidnei J. S. Sant'Anna, *Member* and Alejandro C. Frery, *Member*

Abstract

A new classifier for Polarimetric SAR (PolSAR) images is proposed and assessed in this paper. Its input consists of segments, and each one is assigned the class which minimizes a stochastic distance. Assuming the complex Wishart model, several stochastic distances are obtained from the h - ϕ family of divergences, and they are employed to derive hypothesis test statistics that are also used in the classification process. This article also presents, as a novelty, analytic expressions for the test statistics based on the following stochastic distances between complex Wishart models: Kullback-Leibler, Bhattacharyya, Hellinger, Rényi, and Chi-Square; also, the test statistic based on the Bhattacharyya distance between multivariate Gaussian distributions is presented. The classifier performance is evaluated using simulated and real PolSAR data. The simulated data are based on the complex Wishart model, aiming at the analysis of the proposal well controlled data. The real data refer to the complex L-band image, acquired during the 1994 SIR-C mission. The results of the proposed classifier are compared with those obtained by a Wishart per-pixel/contextual classifier, and we show the better performance of the region-based classification. The influence of the statistical modeling is assessed by comparing the results using the Bhattacharyya distance between multivariate Gaussian distributions for amplitude data. The results with simulated data indicate that the proposed classification method has a very good performance when the data follow the Wishart model. The proposed classifier also performs better than the per-pixel/contextual classifier and the Bhattacharyya Gaussian distance using SIR-C PolSAR data.

Index Terms

Region-Based Classification, Stochastic Distances, Hypothesis Tests, Polarimetry, Wishart distribution

I. INTRODUCTION

The classification of images obtained by polarimetric synthetic aperture radar (PolSAR) sensors is one of the main information extraction techniques from that kind of data. Generally, PolSAR classification falls into three categories: target decomposition [1], PolSAR data statistical modeling [2], and hybrid methods [3], [4], involving both the statistical modeling and target decomposition methods.

Regarding the statistical modeling, the multiplicative model, which takes into account the contributions of both the backscatter and the speckle, has been suitably employed. The return can be modeled by the complex Wishart distribution [5], [6]. Other models have been proposed in the literature for PolSAR data, markedly the

\mathcal{G}_P distribution (which has as particular cases the polarimetric K_P and \mathcal{G}_P^0 distributions [2], [7]), the Gaussian scale mixture [8], [9], generalized complex Gaussian laws [10], and the \mathcal{U} and other models stemming from the multiplicative hypothesis [11]–[14]. These models are more flexible than the Wishart law (they all include the latter as particular case), at the expense of employing additional parameters whose estimation is oftentimes cumbersome.

Several pixel-based classifiers were developed from the Wishart distribution, being one of them the maximum likelihood classifier used in [6] and the unsupervised procedure employed in [15]. Pixel-based classifiers can be improved by the use of spatial context. Frery et al. [2] developed an ICM – Iterative Conditional Modes classifier which employs the maximum likelihood classification result under the complex Wishart distribution as starting point, point wise evidence, and the Potts model as local information. This classifier quantifies the spatial information by a maximum pseudolikelihood estimator in a completely manner as segments do. The Potts model codes the influence of neighboring classes (typically a few, in the implementation here discussed were eight) in a parametric way, whereas a segment is already expected to be a group of data with similar properties. The ICM algorithm proceeds iteratively until convergence, whereas segment classification by distance minimization is a single-step technique.

It is believed that even better PolSAR classification results can be achieved using segmented images (region-based classification). This classification strategy may use a supervised scheme based on stochastic distances between the statistical distributions that model segments and training samples which represent classes. In the case of PolSAR data, these distances must be defined between pairs of complex Wishart distributions.

Salicru et al. [16] developed analytical dissimilarity measures, the so called h - ϕ family of divergences. Hypothesis tests based on statistics derived from these divergences were also developed in [16]. Frery et al. [17], [18] obtained five different distances between complex Wishart distributions: Kullback-Leibler, Bhattacharyya, Hellinger, Rényi and Chi-Square and their corresponding hypothesis tests were also developed and evaluated.

A PolSAR region based classifier using the test statistic derived from the Bhattacharyya stochastic distance between two complex Wishart models was proposed in [19]. The promising results obtained using this classifier in the L band SIR-C image, led us to improve the proposed classifier, by introducing new stochastic distances and their corresponding hypothesis tests. In addition to describing in more details the algorithm developed in [19], this article breaks new ground by presenting analytical expressions for the test statistics based on the following stochastic distances between complex Wishart distributions: Kullback-Leibler, Bhattacharyya, Hellinger, Rényi and Chi-Square, and also the statistic based on the Bhattacharyya distance between multivariate Gaussian distributions. The classifier performance is evaluated using simulated and real PolSAR data. The simulated data is based on the complex Wishart model and the symmetric circularity assumption, aiming at the analysis of such application in statistically well controlled data. The real data refer to the complex L-band image, acquired during the 1994 SIR-C mission.

II. STOCHASTIC DISTANCES AND ASSOCIATED TESTS

Mahalanobis presented the concept of a distance between distributions in the sense that there are pairs of probability laws which are easier to distinguish than others. Such quantities have received a number of denominations

as, for instance, measures of separation, measures of discriminatory information and measures of variation-distance. Many goodness-of-fit tests, such as the likelihood ratio, the chi-square, the score and Wald tests, can be defined in terms of appropriate distance measures between distributions. They all have in common test statistics which increase as the two distributions are further from each other [20].

Salicru et al. [16] proposed the h - ϕ family of divergences as follows. Consider the random variables X and Y defined on the same support S with distributions characterized by the densities $f_X(x; \theta_1)$ and $f_Y(x; \theta_2)$, respectively, where θ_1 and θ_2 are parameters. The h - ϕ divergence between X and Y is given by

$$D_{\phi}^h(X, Y) = h\left(\int_{x \in S} \phi\left(\frac{f_X(x; \theta_1)}{f_Y(x; \theta_2)}\right) f_Y(x; \theta_2) dx\right), \quad (1)$$

where $\phi: (0, \infty) \rightarrow [0, \infty)$ is a convex function and $h: (0, \infty) \rightarrow [0, \infty)$ is a strictly increasing function with $h(0) = 0$ and $h'(x) > 0$ for all $x \in S$. Table I presents the choices of h and ϕ employed in [21] and the divergences they lead to.

TABLE I
(h, ϕ)-DIVERGENCES AND RELATED ϕ AND h FUNCTIONS.

(h, ϕ)-divergence	$h(y)$	$\phi(x)$
Kullback-Leibler	y	$x \log(x)$
Rényi (order $0 < \beta < 1$)	$\frac{1}{\beta-1} \log((\beta-1)y + 1), 0 \leq y < \frac{1}{1-\beta}$	$\frac{x^{\beta} - \beta(x-1) - 1}{\beta-1}, 0 < \beta < 1$
Hellinger	$y/2, 0 \leq y < 2$	$(\sqrt{x} - 1)^2$
Bhattacharyya	$-\log(-y + 1), 0 \leq y < 1$	$-\sqrt{x} + \frac{x+1}{2}$
χ^2	$y/4$	$(x-1)^2(x+1)/x$

These h - ϕ divergences are not granted to be symmetric, so they are not necessarily distances. A simple way to overcome this is computing

$$d_{\phi}^h(X, Y) = \frac{D_{\phi}^h(X, Y) + D_{\phi}^h(Y, X)}{2}, \quad (2)$$

regardless whether $D_{\phi}^h(\cdot, \cdot)$ is symmetric or not. Furthermore, if X and Y obey the same distribution with possibly only different parameters, it is enough to write $d_{\phi}^h(\theta_1, \theta_2)$. Doing so, it is granted that $d_{\phi}^h(\theta_1, \theta_2) = 0$ if and only if $\theta_1 = \theta_2$ and that $d_{\phi}^h(\theta_1, \theta_2) \geq 0$, but how big this quantity is has no immediate interpretation.

Salicru et al. [16] provided a means to transform distances into test statistics with known asymptotic properties. Let $\widehat{\theta}_1$ and $\widehat{\theta}_2$ be maximum likelihood estimators of θ_1 and θ_2 based on samples of sizes m and n , respectively. The parameter space is $\Theta \subset \mathbb{R}^M$. Under the null hypothesis $H_0: \theta_1 = \theta_2$, the test statistic

$$S_{\phi}^h = \frac{2mn}{m+n} \frac{d_{\phi}^h(\widehat{\theta}_1, \widehat{\theta}_2)}{h'(0)\phi''(1)} \quad (3)$$

converges in distribution to a χ_M^2 distributed random variable, where M is the number of parameters of the model, provided $m, n \rightarrow \infty$ such that $m/(m+n) \rightarrow \lambda \in (0, 1)$.

Nascimento et al. [21] derived h - ϕ tests for the \mathcal{G}^0 model for intensity SAR data and used them for the discrimination of targets in remote sensing images. Cintra et al. [22] compared those tests with the Kolmogorov-Smirnov test, and verified their robustness. Frery et al. [17] derived these tests for polarimetric SAR data under the Wishart model. These last results will be recalled in the next section.

III. TESTS BASED ON STOCHASTIC DISTANCES BETWEEN MODELS

The Wishart law is widely accepted as a model for PolSAR data, mainly on homogeneous areas. This model stems from the multilook processing of data which obey the complex Gaussian distribution.

We may consider systems with q polarization elements, which record the complex Gaussian distributed random vector $\mathbf{y} = (S_1 \ S_2 \ \cdots \ S_q)^T$, where ' T ' denotes vector transposition. This distribution is characterized by its complex covariance matrix $\Sigma = E(\mathbf{y}\mathbf{y}^*)$, where ' $*$ ' denotes the complex conjugate transpose, and $E(\cdot)$ is the statistical expectation operator. In order to enhance the signal-to-noise ratio, L independent and identically distributed samples are usually averaged to form the L -looks covariance matrix:

$$\mathbf{Z} = \frac{1}{L} \sum_{i=1}^L \mathbf{y}_i \mathbf{y}_i^*. \quad (4)$$

Under these hypotheses, \mathbf{Z} follows a scaled complex Wishart distribution with parameters Σ and L (denoted by $\mathbf{Z} \sim \mathcal{W}(\Sigma, L)$), and characterized by the following probability density function:

$$f_{\mathbf{Z}}(\mathbf{Z}; \Sigma, L) = \frac{L^q |\mathbf{Z}|^{L-q}}{|\Sigma|^L \Gamma_q(L)} \exp(-L \operatorname{tr}(\Sigma^{-1} \mathbf{Z})), \quad (5)$$

where $\Gamma_q(L) = \pi^{q(q-1)/2} \prod_{i=0}^{q-1} \Gamma(L-i)$, $L \geq q$, $\Gamma(\cdot)$ is the gamma function, and $\operatorname{tr}(\cdot)$ is the trace operator. It is important to observe that this Wishart distribution satisfies $E(\mathbf{Z}) = \Sigma$. The maximum likelihood estimator of Σ , based on N independent samples, is the sample mean $\hat{\Sigma} = N^{-1} \sum_{i=1}^N \mathbf{Z}_i$, and L can be estimated by any of the techniques discussed in [23].

Frery et al. [17] computed stochastic distances between complex Wishart distributions based on the h - ϕ divergences presented in Table I, in their most general form (different covariance matrices and number of looks). In the following we derive the test statistics for the case of same number of looks L , assumed known. The null hypothesis under which these statistics follow a χ^2 distribution is $H_0 : \Sigma_1 = \Sigma_2$.

$$S_{\text{KL}}(\widehat{\Sigma}_1, \widehat{\Sigma}_2) = \frac{2mn}{m+n} L \left[\frac{\text{tr}(\widehat{\Sigma}_1^{-1} \widehat{\Sigma}_2 + \widehat{\Sigma}_2^{-1} \widehat{\Sigma}_1)}{2} - q \right]. \quad (6)$$

$$S_{\text{B}}(\widehat{\Sigma}_1, \widehat{\Sigma}_2) = \frac{8mn}{m+n} L \left[\frac{\log |\widehat{\Sigma}_1| + \log |\widehat{\Sigma}_2|}{2} - \log \left| \left(\frac{\widehat{\Sigma}_1^{-1} + \widehat{\Sigma}_2^{-1}}{2} \right)^{-1} \right| \right]. \quad (7)$$

$$S_{\text{H}}(\widehat{\Sigma}_1, \widehat{\Sigma}_2) = \frac{8mn}{m+n} \left\{ 1 - \left[\frac{2^{-1}(\widehat{\Sigma}_1^{-1} + \widehat{\Sigma}_2^{-1})^{-1}}{\sqrt{|\widehat{\Sigma}_1| |\widehat{\Sigma}_2|}} \right]^L \right\}. \quad (8)$$

$$S_{\text{R}}^{\beta}(\widehat{\Sigma}_1, \widehat{\Sigma}_2) = \frac{2mn}{\beta(m+n)} \left\{ \frac{\log 2}{1-\beta} + \frac{1}{\beta-1} \log \left\{ \begin{aligned} & [|\widehat{\Sigma}_1|^{-\beta} |\widehat{\Sigma}_2|^{\beta-1} |(\beta \widehat{\Sigma}_1^{-1} + (1-\beta) \widehat{\Sigma}_2^{-1})^{-1}|]^L \\ & + [|\widehat{\Sigma}_1|^{\beta-1} |\widehat{\Sigma}_2|^{-\beta} |(\beta \widehat{\Sigma}_2^{-1} + (1-\beta) \widehat{\Sigma}_1^{-1})^{-1}|]^L \end{aligned} \right\} \right\}. \quad (9)$$

$$S_{\chi^2}(\widehat{\Sigma}_1, \widehat{\Sigma}_2) = \frac{mn}{2(m+n)} \left[\left(\frac{|\widehat{\Sigma}_1|}{|\widehat{\Sigma}_2|^2} \text{abs}(|(2\widehat{\Sigma}_2^{-1} - \widehat{\Sigma}_1^{-1})^{-1}|) \right)^L + \left(\frac{|\widehat{\Sigma}_2|}{|\widehat{\Sigma}_1|^2} \text{abs}(|(2\widehat{\Sigma}_1^{-1} - \widehat{\Sigma}_2^{-1})^{-1}|) \right)^L - 2 \right], \quad (10)$$

where ‘abs’ denotes absolute value. Equations (6), (7), (8), (9) and (10) are, respectively, the Kullback-Leibler, Bhattacharyya, Hellinger, Rényi of order β and χ^2 test statistics based on stochastic distances. Each test rejects the null hypothesis at level $1 - \alpha$ if $\Pr(\chi_{q^2}^2 \geq s_{\phi}^h) \leq \alpha$, where $\chi_{q^2}^2$ follows a χ^2 distribution with q^2 degrees of freedom.

Notice that Equations (6)–(10) rely on two simple operations on complex matrices: the inverse and the determinant.

Oftentimes complete PolSAR data are not available. For instance, Radarsat-2 provides the HH, VV, HV and VH intensities, while dual polarizations are available from Envisat (HH–HV or VV–VH) and Cosmos Skymed (HH–HV or HH–VV). In these cases, only elements of the main diagonal of L -looks covariance matrix \mathbf{Z} are provided. Multivariate Gamma models for these data can be derived as marginal distribution from the scaled complex Wishart law characterized by the density given in equation (5). In practice, such marginal distributions are available for both the bivariate and trivariate cases. The bivariate case, cf. [24, Eq. (30)] was used in a maximum likelihood classification algorithm for dual intensity SAR data in [25]. Hagedorn et al. [26] derived both the bi- and tri-variate χ^2 distributions of diagonal elements of a Wishart law, but there are currently no expressions available for the distances between these multivariate chi-squared distributions.

Additionally, an increased number of looks and the amplitude format yield a distribution which can be approximated by a multivariate Gaussian law. This, and the fact that multivariate Gaussian classifiers are a commodity of image processing software, suggests the use of the Gaussian model as a testbed for the data here considered.

Theodoridis and Koutroumbas [27] compute stochastic distances under the q -variate Gaussian model. Using these

results and equation (3), we derived the Bhattacharyya test statistic for the null hypothesis $H_0 : (\boldsymbol{\mu}_1, \boldsymbol{\Sigma}_1) = (\boldsymbol{\mu}_2, \boldsymbol{\Sigma}_2)$:

$$T_B = \frac{8mn}{m+n} \left[[(\widehat{\boldsymbol{\mu}}_1 - \widehat{\boldsymbol{\mu}}_2)^T \left(\frac{\widehat{\boldsymbol{\Sigma}}_1 + \widehat{\boldsymbol{\Sigma}}_2}{2} \right)^{-1} (\widehat{\boldsymbol{\mu}}_1 - \widehat{\boldsymbol{\mu}}_2)] + 4 \log \frac{|\frac{\widehat{\boldsymbol{\Sigma}}_1 + \widehat{\boldsymbol{\Sigma}}_2}{2}|}{\sqrt{|\widehat{\boldsymbol{\Sigma}}_1| |\widehat{\boldsymbol{\Sigma}}_2|}} \right], \quad (11)$$

where $\widehat{\boldsymbol{\mu}}_i$ and $\widehat{\boldsymbol{\Sigma}}_i$ are the maximum likelihood estimators of the mean vector and the covariance matrix, $i = 1, 2$. The null hypothesis is rejected at level $1 - \alpha$ if $\Pr(\chi_{q(q+3)/2}^2 \geq T_B) \leq \alpha$, where $\chi_{q(q+3)/2}^2$ follows a χ^2 distribution with $q(q+3)/2$ degrees of freedom.

IV. REGION CLASSIFICATION BASED ON TEST STATISTICS

In this section we define the two classification products we obtain using test statistics based on stochastic distances: minimum test statistics and p -value maps.

Assume the image support is partitioned in r disjoint segments C_1, \dots, C_r . The PolSAR data from each segment is denoted Z_{C_i} , $1 \leq i \leq r$, and a covariance matrix $\widehat{\boldsymbol{\Sigma}}_i$ is estimated with these data by maximum likelihood. The user provides k prototypes in the form of samples (supervised scheme), with which covariance matrices $\widehat{\boldsymbol{\Sigma}}_\ell$, $1 \leq \ell \leq k$, are estimated by maximum likelihood. The purpose is to classify each segment C_i in one of the k prototypes.

Compute the $r \times k$ test statistics which contrast the null hypothesis $H_0 : \boldsymbol{\Sigma}_i = \boldsymbol{\Sigma}_\ell$ with one of the equations given in (6)–(10) for every segment $1 \leq i \leq r$ and every prototype $1 \leq \ell \leq k$. The classification based on minimum test statistic consists of assigning the segment C_i to the class represented by prototype t if

$$S_\phi^h(\widehat{\boldsymbol{\Sigma}}_i, \widehat{\boldsymbol{\Sigma}}_t) < S_\phi^h(\widehat{\boldsymbol{\Sigma}}_i, \widehat{\boldsymbol{\Sigma}}_\ell) \quad (12)$$

for every $t \neq \ell$. Once the segment C_i has been assigned to the class represented by prototype t , the p -value of the assignment is computed as

$$p_{i,t} = \Pr(\chi_\nu^2 > s_\phi^h(\widehat{\boldsymbol{\Sigma}}_i, \widehat{\boldsymbol{\Sigma}}_t)), \quad (13)$$

where ν is the numbers of parameters of the considered model: $\nu = q^2$ for the Wishart distribution, and $\nu = q(q+3)/2$ for the q -variate Gaussian distribution. This value gives an idea of the confidence of the decision.

The rule given by inequality (12) opens a number of interesting alternatives, among them, instead of choosing **one** test statistic, use all available ones. Each test statistic will provide a class for each segment, and these classifications can be fused by majority vote. The information provided by equation (13) can also be used; a fuzzy classification can be made for each segment to **all** the classes whose p -value is above a certain threshold.

V. APPLICATION TO POLSAR DATA

The classification procedure described in Section IV was applied and evaluated under two approaches: using simulated data, which was generated under the complex Wishart distribution, and using a real SIR-C full PolSAR image, in L-band.

A. SIR-C Polarimetric Data Description

The SIR-C full polarimetric image is from an agricultural area located in Petrolina city, Northeast of Brazil. Table II presents the study area location and the basic characteristics of the SIR-C image. The main observed land cover classes are River, Caatinga, Prepared Soil, Soybean in three different phenological stages, Tillage, and Corn in two phenological stages. The training and test samples for these classes are shown in Figures 1(a) and 1(b), and their legends in Figure 1(c). These samples were properly sub-sampled to diminish the pixels correlation influence, and their final sizes are shown in Table III.

TABLE II
SIR-C IMAGE AND STUDY AREA INFORMATION.

Study area location	09° 07' S, 40° 18' W (central coordinate), about 40 km northeast of the city of Petrolina-PE, Brazil
Aquisition date	April 14 th , 1994
Image size (pixels)	407 × 370
Nominal number of looks	4.785
Frequency	L-band - 1.254 GHz
Pixel spacing	12.5m × 12.5m
Incidence angle	49.496°
Orbit direction	Descending

TABLE III
TRAINING AND TEST SAMPLES DESCRIPTION.

Class	Description	# Training samples	# Test samples
River	Water body	1192	976
Caatinga	A stepped vegetation composed of stunted trees and thorny bushes, found in areas of little rainfall in Brazil	1006	820
Prepared Soil	Soil ready for seeding	715	442
Soybean 1	Soybean with approximately 52 days after seeding	212	99
Soybean 2	Soybean with approximately 66 days after seeding	174	117
Soybean 3	Soybean with approximately 113 days after seeding	390	216
Tillage	Agricultural crops residuals	181	98
Corn 1	Corn with less than 124 days after seeding	661	364
Corn 2	Corn with approximately 133 days after seeding	191	77

Frery et al. [2] concluded that, with the exception of the class “River”, the samples presented in Fig. 1 depart from the Wishart distribution [2, page. 7, Table III] and are better explained by the \mathcal{K}_P and \mathcal{G}_P^0 distributions. As previously mentioned, there are no analytic expressions for the stochastic distances between such generalized models, and numerical integration would be unfeasible due the need to integrate on the domain of all positive

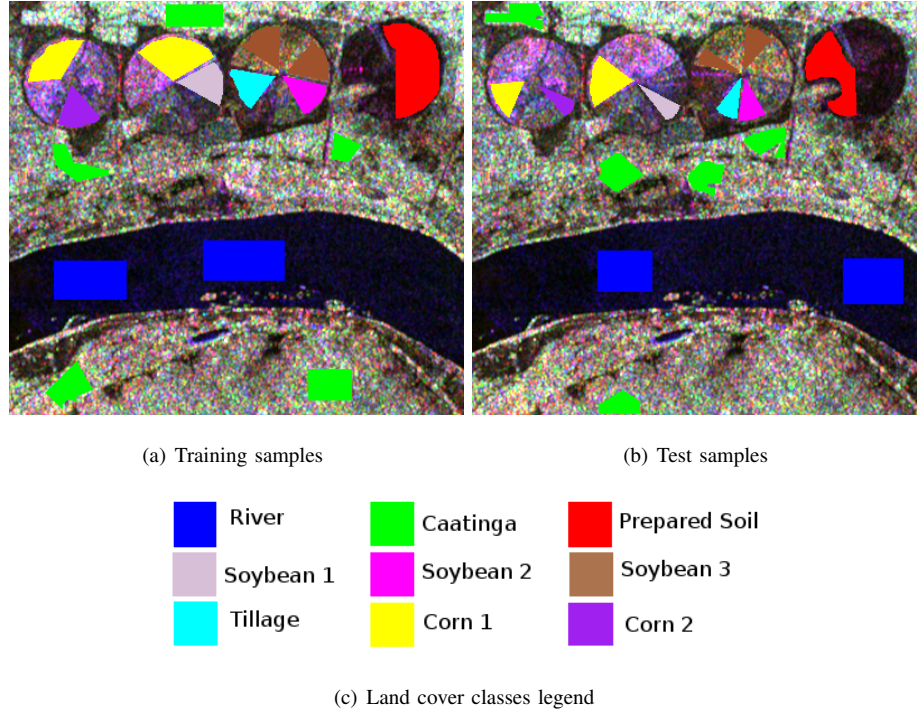


Fig. 1. L-band SIR-C intensity images (HH(R), HV(G), VV(B)) and location of training and test samples.

definite Hermitian matrices. In this manner, although the exact description of the data could be improved, adopting the Wishart model still leads to interesting results.

B. Simulated Data Description

Simulated data were generated under the symmetric circularity assumption [5]. The simulation aims at obtaining random covariance matrices realizations under the complex Wishart distribution with a fixed number of looks (L). Initially, single-look polarimetric SAR data, represented by the q -variate complex Gaussian random vector \mathbf{y}_q , are generated. Assuming that \mathbf{y}_q follows a q -variate complex Gaussian distribution with zero mean and covariance matrix Σ_q (denoted $\mathbf{y}_q \sim \mathcal{CN}_q(0, \Sigma_q)$), the simulation is performed by first sampling a $2q$ -variate vector \mathbf{x} such that $\mathbf{x}_{2q} \sim \mathcal{N}_{2q}(0, \Sigma_{2q}^*)$, where, under the symmetric circular assumption and according to [5] and [28], Σ_{2q}^* is such that:

$$\Sigma_{2q}^* = \frac{1}{2} \begin{bmatrix} \Re(\Sigma_q) & -\Im(\Sigma_q) \\ \Im(\Sigma_q) & \Re(\Sigma_q) \end{bmatrix},$$

where \Re and \Im denote the real and imaginary parts of a complex number, respectively. The first q elements of \mathbf{x}_{2q} become the real parts of the elements in the complex vector \mathbf{y}_q and the last q elements of \mathbf{x}_{2q} become the imaginary parts of the elements in the complex vector \mathbf{y}_q . This process is repeated as many times as the required number of samples, where each sample represents a polarimetric pixel of an image. The L -looks complex covariance matrix image is obtained according to equation (4).

The simulation process described above was used to produce images representing the nine classes observed in the SIR-C L-band PolSAR image. The covariance matrices for each class were the estimated covariance matrices, using the training samples presented in Figure 1(a), whose numbers of pixels are shown in Table III. These covariance matrices are presented in equations (14)–(22) of the appendix. The simulation was performed with four looks and three polarization bands, HH, HV and VV. The simulated covariance matrix image of each class has 150×150 pixels. A final image was generated by mosaicking the simulated images of the individual classes. This final image has 450×450 pixels, i.e., the images were grouped in a 3×3 images classes configuration. An RGB color composition of the intensities bands from the covariance matrix image is shown in Figure 2.

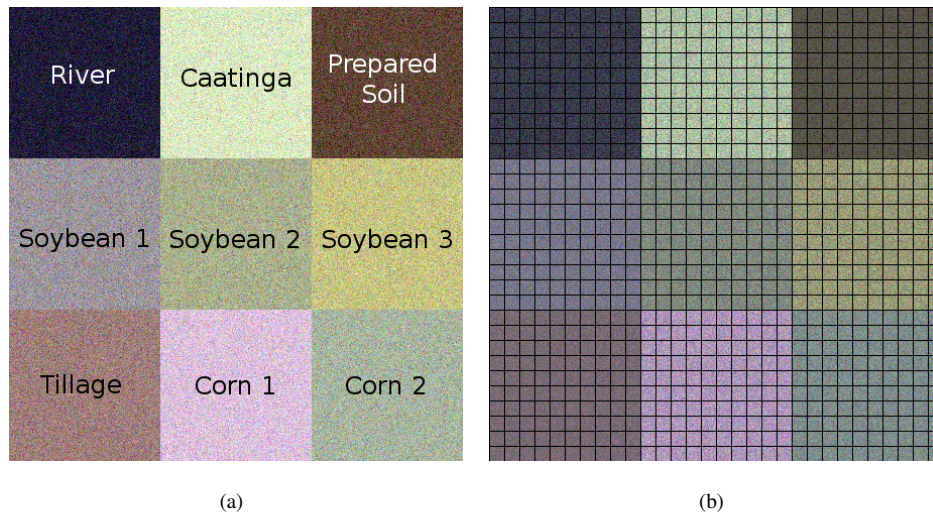


Fig. 2. Simulated PolSAR image: (a) intensities color composition - HH(R), HV(G), VV(B) and (b) segmentation scheme in 15×15 pixels segments.

The region classification procedure was applied using four different segmentation procedures to all the segments of sizes 5×5 , 10×10 , 15×15 and 30×30 pixels, respectively. The 15×15 segmented image is presented in Figure 2(b). The prototype of each class, also needed for the classification procedure, was generated by sampling 900 pixels, representing a training sample of 30×30 pixels for each class. The simulation of the prototypes, performed independently of the simulated image, ensures that identical data are not being considered in the computation of test statistics and, consequently, in the determination of the corresponding p -values.

C. Assessing the Classification Procedure using Simulated Data

The region-based classifications of the simulated data, using stochastic distances and the minimum test statistics given in equation (12), aimed at the evaluation of the classification procedure under rigorous well controlled statistical model, as the data was simulated considering the complex Wishart distribution. An additional classification result was obtained, considering the multivariate Gaussian model for the multivariate amplitude image obtained from the simulated PolSAR image. For this case, the analytic expression for the Bhattacharyya test statistic showed in equation (11) was used.

Observing that we have four segmented images and six stochastic distances (five from Wishart and one from Gaussian models), twenty four classified images were produced. The classifications performed on segments of sizes 10×10 , 15×15 and 30×30 pixels were 100% correct. The classifications of segments of size 5×5 pixels reached a global accuracy of 99.81% for the Bhattacharyya, Kullback-Leibler, Hellinger and Rényi distances, and 99.58% for the χ^2 distance. Errors occurred in segments belonging to the simulated classes of Soybean 2 and Corn 2.

These results show the high quality of the proposed classifier when the assumptions of the data distribution are satisfied, especially for segments with large amounts of pixels (equal or greater than 100 pixels).

Figure 3 shows the classified images using the six stochastic distances, for the case of 5×5 pixels segments. The slight confusion between the Soybean 2 and Corn 2 classes can be observed in this figure, as well as with some segments of the Caatinga class, classified as Corn 1 class under the χ^2 distance. Under the Gaussian model, the global accuracy was 98.35% for the Bhattacharyya distance. A higher confusion between Soybean 2 and Corn 2 classes was observed when compared with the results obtained by the classifiers that adopt the Wishart model, a result which stresses the importance of using the proper distribution to model the data.

For each classification result, a map of the p -values of the test statistics, an indicator of the confidence of the assignment decision, was also produced. These results are presented in Figure 4, where the white positions mark those segments for which the null hypothesis (the equality between the covariance matrices of the segment and of the assigned prototype) was not rejected at the 5 % significance level. The percentages of these segments for each sample size and each distance is presented in Table IV.

TABLE IV
PERCENTAGE OF SEGMENTS FOR WHICH H_0 WAS NOT REJECTED AT 5 % SIGNIFICANCE LEVEL, FOR SIMULATED DATA CASE.

Distances	Percentage (%)			
	5×5 pixels	10×10 pixels	15×15 pixels	30×30 pixels
	8100 segments	2025 segments	900 segments	225 segments
Bhattacharyya	94.0	95.2	94.3	93.8
Kullback-Leibler	93.7	95.1	94.3	93.3
Hellinger	95.2	95.3	94.8	93.8
Rényi (order $\beta = 0.9$)	93.8	95.1	94.3	93.8
χ^2	75.5	91.2	92.8	92.4
Bhattacharyya (Gaussian)	90.6	94.1	95.1	98.2

The results presented in Figure 4 and in Table IV are compatible with the theoretically expected values. The hypothesis tests rejection rates were approximately 5% for all segmentation cases and stochastic distances, except when the χ^2 distance was used, and the Bhattacharyya Gaussian distance was applied to small (5×5 pixels) segments. The rejection rates for the χ^2 distance were higher than the theoretical values in all segmentation cases, reaching the value of approximately 24.5% for the segmentation of 5×5 pixels segments. The poor performance of the χ^2 distance test statistic was also observed by [17], where this big test size was first described.

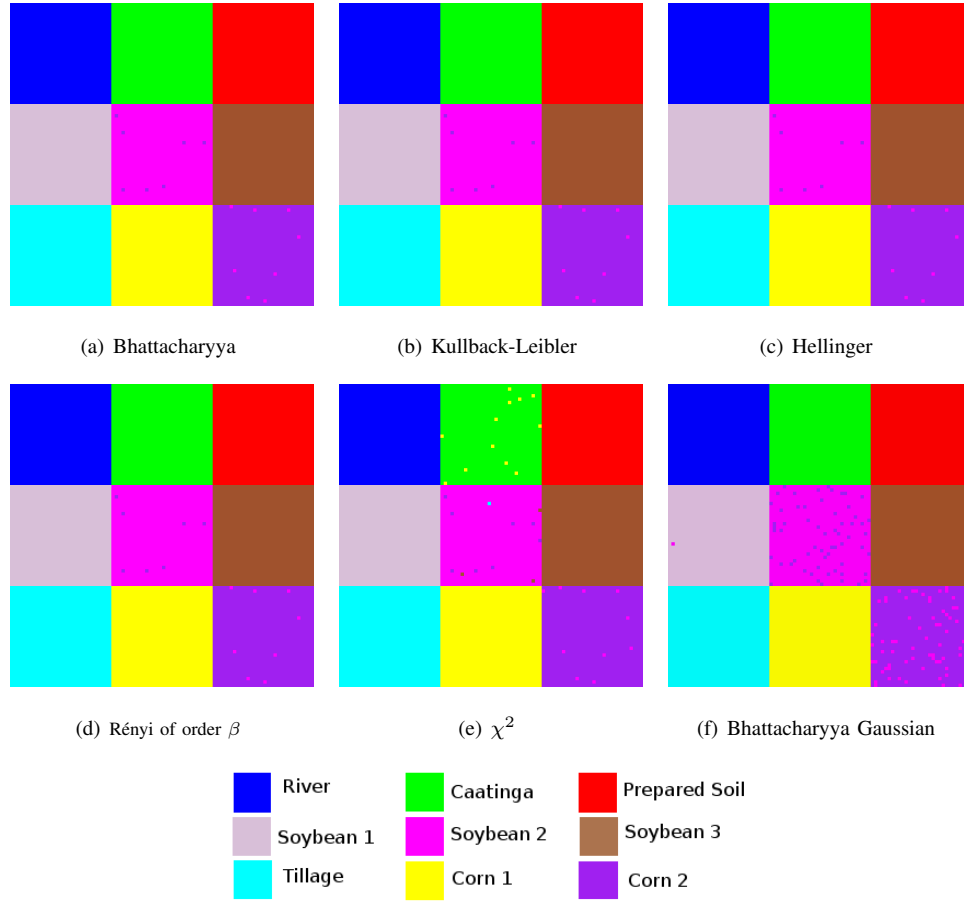


Fig. 3. Classification results of the simulated data for segments of size 5×5 pixels.

The rejection rate of the Hellinger distance is 5% in 5×5 , 10×10 and 15×15 pixels segments, while the Bhattacharyya Gaussian distance reaches this rate only in large segments (15×15 and 30×30), as expected according to the Central Limit Theorem.

D. Assessing the Classification Procedure using SIR-C Polarimetric Image

Prior to classification, the SIR-C image was segmented using the SegSAR software [29]: a hierarchical multi-level region growing segmentation algorithm designed for intensity SAR data which uses tests based on the Gamma and Gaussian distributions. The SegSAR parameters used for segmentation were 100 pixels of minimum area, and 1 dB of similarity.

The equivalent number of looks value was estimated considering all polarization channels using the method described in [2], which is also referred by Anfisen et al. [23] as Fractional Moment Estimate; the computed value was 2.97. The segmented image is presented in Figure 5(a); each segment is shown in a color defined by associating the RGB channels to the means of each intensity polarization (HH, HV and VV). The classification procedure

described by equation (12) was applied for L-band SIR-C data using this segmented image. The tests statistics are given in equations (6)–(10), assuming the Wishart law, as well as equation (11), assuming the Gaussian law for amplitude data. The p -value map, defined in equation (13), was computed for every segment in each classification.

The region classifications were also compared to the contextual ICM polarimetric classification described in [2], which is also based on the Wishart distribution. Therefore, six region classifications and one ICM classification were obtained. The classification performances were compared using the estimated Kappa coefficient of agreement ($\hat{\kappa}$), and the overall accuracy, as formulated in [30].

The classifications results are presented in Figure 5. The overall accuracy, the estimated Kappa coefficient of agreement and its variance for all classifications are presented in Table V. The tests for equality of Kappa showed that the classifications based on Kullback-Leibler, Bhattacharrya, Hellinger and Rényi distances between Wishart distributions produced statistically similar results. The contextual classification is only superior to the χ^2 distance classification, which is the worst stochastic distance-based classification, in agreement with the results found with simulated data. The classification based on the Bhattacharrya Gaussian distance is only superior to the contextual and to the χ^2 distance classification.

Table VI presents, for each stochastic distance, the percentage of segments with p -value greater than 0.05, i.e., the percentage of segments that were not rejected at this level. These segments are illustrated in white in Figure 6.

Although the values of Table V showed promising results for minimum distance classification using complex Wishart distributions, the percentages showed in Table VI are far from the theoretical 95%.

TABLE V
ASSESSMENT OF CLASSIFICATION RESULTS FOR L-BAND SIR-C IMAGE.

Classification Method		L-band SIR-C Image		
		Overall Accuracy (%)	$\hat{\kappa}$	$s_{\hat{\kappa}} (\times 10^{-5})$
Region-based	Bhattacharrya	86.60	0.8346	1.253
	Kullback-Leibler	86.60	0.8346	1.253
	Hellinger	85.97	0.8269	1.296
	Rényi (order $\beta = 0.9$)	86.60	0.8346	1.253
	χ^2	71.36	0.6544	2.081
	Bhattacharrya (Gaussian)	85.35	0.8191	1.333
Contextual	ML/ICM - Wishart	83.97	0.8025	1.430

VI. CONCLUSIONS AND FUTURE WORK

A new region-based classifier for PolSAR data using stochastic distances between complex Wishart distributions and derived hypothesis tests was presented. The proposed classifier was applied to simulated data and to a real L-band PolSAR image from the SIR-C mission.

TABLE VI
PERCENTAGE OF SEGMENTS OF THE SIR-C L-BAND IMAGE THAT WERE NOT REJECTED AT THE 5 % SIGNIFICANCE LEVEL.

Distances	Percentage (%)
Bhattacharrya	9.76
Kullback-Leibler	9.58
Hellinger	10.49
Rényi (order $\beta = 0.9$)	9.58
χ^2	6.33
Bhattacharrya (Gaussian)	6.33

The classification results using simulated PolSAR data based on the complex Wishart model obtained an overall accuracy of 100%, with the exception of few misclassification observed when small segments (5×5 pixels) were used. The acceptance rates of the null hypothesis tests, which measures the confidence of the classification assignments, obtained very close values to the theoretically expected ones for almost all distances and segment sizes. The poorest results occurred when the χ^2 distance was used, especially in the classifications of small segments. With the exception of this last case, the evidence allows us to conclude that the proposed classification method has a very good performance and confidence when the data rigorously follow the Wishart model. Further evaluations with non-perfect Wishart independent observations, such as under presence of noise, departures from the pure model, and spatial correlation are under implementation and investigation.

The use of statistic based on the Hellinger distance between Wishart laws usually outperforms the results obtained by other distances, specially for segmented images with small regions. This may be due to the robustness which the procedures derived from this distance have. The Battacharrya Gaussian distance is also a good option for images having large segments.

The proposed region-based classifier, when applied to L-band PolSAR data from the SIR-C mission, obtained also very good performance in terms of overall accuracy and κ coefficient of agreement. The best results were obtained with the Bhattacharrya, Kullback-Leibler, Rényi and Hellinger distances between Wishart distributions. The results using these distances overcame the classification results obtained using multivariate amplitude data and the Bhattacharrya distance between Gaussian laws. This evidence proves the relevance of using appropriate modeling of the data when employing stochastic distances.

In comparison with a contextual Maximum Likelihood/ICM classifier [2], the new classifier obtained also better results, with statistically superior κ values. Such improvement can also be observed by examining the huge amount of undesirable small areas that still exist in the contextual result, while those artifacts are minimized by the region-based classification.

The rejection rates of the null hypothesis tests concerning the real PolSAR data was distant from the theoretical expected values, achieving values higher than 90%. Since the results with complex Wishart simulated data were perfectly compatible with the theoretical expected significance level, this poor result with real data may be due

to a less than optimal description of the real data by the theoretical model. As mentioned before, many samples are better modeled by more general distributions as the \mathcal{K}_P and \mathcal{G}_P^0 laws. These results suggest that the proposed method is robust with respect to the classification map, but not the map of p -values.

Another possible sources of misfit are spatial correlation, which alters the effective sample sizes in Eq. (3), the existence of more classes than those identified by the expert, the large size of some segments (as in the “River” class), and the influence of an inadequate segmentation (the SegSAR algorithm used in this paper was developed for intensity and not for PolSAR data). Further investigation must be taken forward with real data examples in order to clarify the possible vulnerability of hypothesis testing due to these possibilities.

The analysis of the proposed region-based classification led us to conclude that the classifier has great potential for PolSAR data analysis. It is noteworthy that the expressions that have to be computed rely on simple operations on matrices: the determinant and the inverse. In the future, further investigation will be conducted using also the classifier module considering the intensity pair distribution for bivariate intensity data, a common SAR data availability situation commented in Section III.

Recent research [31], [32] reports interesting results with the use of the Geodesic Rao metric [33]. This, and other tests statistics for hypothesis testing PolSAR data distributions, along with improved [34]–[36] and robust [37], [38] estimation in models which incorporate texture [7], [39] are future lines of research.

APPENDIX

The covariance matrices of the nine classes of the SIR-C images were estimated by maximum likelihood using the selected training samples (Figure 1(a) and Table III). Equations (14) to (22) present the estimated covariance matrices for the following classes: River, Caatinga, Prepared Soil, Soybean 1, Soybean 2, Soybean 3, Tillage, Corn 1, and Corn 2, respectively. These matrices were the parameter used for image simulation under the Wishart model, as described in section V-B. Only the upper triangle and the diagonal are displayed in the equations (14) to (22) because the covariance matrix (Σ) is Hermitian and, therefore, the remaining elements are the complex conjugates.

REFERENCES

- [1] J. S. Lee and E. Pottier, *Polarimetric radar imaging*, CRC Press, 1 edition, 2008.
- [2] A. C. Frery, A. H. Correia, and C. C. Freitas, “Classifying multifrequency fully polarimetric imagery with multiple sources of statistical evidence and contextual information,” *IEEE Transactions on Geoscience and Remote Sensing*, vol. 45, no. 10, pp. 3098–3109, Oct. 2007.
- [3] J.-S. Lee, M. R. Grunes, T. L. Ainsworth, L.-J. Du, D. L. Schuler, and S. R. Cloude, “Unsupervised classification using polarimetric decomposition and the complex Wishart classifier,” *IEEE Transactions on Geoscience and Remote Sensing*, vol. 37, no. 5, pp. 2249–2258, sep 1999.
- [4] L. Ferro-Famil, E. Pottier, and J.-S. Lee, “Unsupervised classification of multifrequency and fully polarimetric SAR images based on the H/A/Alpha-Wishart classifier,” *IEEE Transactions on Geoscience and Remote Sensing*, vol. 39, no. 11, pp. 2332–2342, nov 2001.
- [5] J. W. Goodman, “Statistical analysis based on a certain multivariate complex gaussian distribution (an introduction),” *Annals of Mathematical Statistics*, vol. 34, no. 1, pp. 152–177, 1963.
- [6] J.-S. Lee, M. R. Grunes, and R. Kwok, “Classification of multi-look polarimetric SAR imagery based on complex Wishart distribution,” *International Journal of Remote Sensing*, vol. 15, no. 11, pp. 2299–2311, February 1994.

- [7] C. C. Freitas, A. C. Frery, and A. H. Correia, "The polarimetric \mathcal{G} distribution for SAR data analysis," *Environmetrics*, vol. 16, no. 1, pp. 13–31, 2005.
- [8] A. P. Doulgeris, S. N. Anfinsen, and T. Eltoft, "Classification with a non-Gaussian model for PolSAR data," *IEEE Transactions on Geoscience and Remote Sensing*, vol. 46, no. 10, pp. 2999–3009, oct. 2008.
- [9] A. Doulgeris and T. Eltoft, "Scale mixture of gaussian modelling of polarimetric SAR data," *EURASIP Journal on Advances in Signal Processing*, vol. 2010, pp. 874592, 2010.
- [10] M. Novey, T. Adali, and A. Roy, "A complex generalized Gaussian distribution: Characterization, generation, and estimation," *IEEE Transactions on Signal Processing*, vol. 58, no. 3, pp. 1427–1433, march 2010.
- [11] G. Vasile, F. Pascal, J.-P. Ovarlez, P. Formont, and M. Gay, "Optimal parameter estimation in heterogeneous clutter for high-resolution polarimetric SAR data," *IEEE Geoscience and Remote Sensing Letters*, vol. 8, no. 6, pp. 1046–1050, nov. 2011.
- [12] L. Bombrun, G. Vasile, M. Gay, and F. Totir, "Hierarchical segmentation of polarimetric SAR images using heterogeneous clutter models," *IEEE Transactions on Geoscience and Remote Sensing*, vol. 49, no. 2, pp. 726–737, feb. 2011.
- [13] S. Khan and R. Guida, "On single-look multivariate \mathcal{G} distribution for PolSAR data," *IEEE Journal of Selected Topics in Applied Earth Observations and Remote Sensing*, vol. 5, no. 4, pp. 1149–1163, aug. 2012.
- [14] S. N. Anfinsen, A. P. Doulgeris, and T. Eltoft, "Goodness-of-fit tests for multilook polarimetric radar data based on the Mellin transform," *IEEE Transactions on Geoscience and Remote Sensing*, vol. 49, no. 7, pp. 2764–2781, july 2011.
- [15] D. K. Atwood, D. Small, and R. Gens, "Improving PolSAR land cover classification with radiometric correction of the coherency matrix," *IEEE Journal of Selected Topics in Applied Earth Observations and Remote Sensing*, vol. 5, no. 3, pp. 848–856, 2012.
- [16] M. Salicru, D. Morales, M. L. Menendez, and L. Pardo, "On the applications of divergence type measures in testing statistical hypotheses," *Journal of Multivariate Analysis*, vol. 51, no. 2, pp. 372–391, November 1994.
- [17] A. C. Frery, A. D. C. Nascimento, and R. J. Cintra, "Information theory and image understanding: An application to polarimetric SAR imagery," *Chilean Journal of Statistics*, vol. 2, no. 2, pp. 81–100, 2011.
- [18] A. C. Frery, A. D. C. Nascimento, and R. J. Cintra, "Hypothesis test in complex Wishart distributions," in *Proceedings of 5th International Workshop on Science and Applications of SAR Polarimetry and Polarimetric Interferometry, POLinSAR 2011*, Frascati, Italy, January 2011.
- [19] W. B. Silva, A. C. Frery, C. C. Freitas, and S. J. S. Sant'Anna, "PolSAR region classifier based on stochastic distances and hypothesis tests," in *2012 IEEE International Geoscience and Remote Sensing Symposium (IGARSS)*, july 2012.
- [20] L. P. Llorente, *Statistical Inference Based on Divergence Measures*, Statistics, Textbooks and Monographs. Chapman & Hall/CRC, 2006.
- [21] A. D. C. Nascimento, R. J. Cintra, and A. C. Frery, "Hypothesis testing in speckled data with stochastic distances," *IEEE Transactions on Geoscience and Remote Sensing*, vol. 48, no. 1, pp. 373–385, 2010.
- [22] R. J. Cintra, A. C. Frery, and A. D. C. Nascimento, "Parametric and nonparametric tests for speckled imagery," *Pattern Analysis and Applications*, in press.
- [23] S. N. Anfinsen, A. P. Doulgeris, and T. Eltoft, "Estimation of the equivalent number of looks in polarimetric synthetic aperture radar imagery," *IEEE Transactions on Geoscience and Remote Sensing*, vol. 47, no. 11, pp. 3795–3809, 2009.
- [24] J.-S. Lee, K. W. Hoppel, S. A. Mango, and A. R. Miller, "Intensity and phase statistics of multilook polarimetric and interferometric SAR imagery," *IEEE Transactions on Geoscience and Remote Sensing*, vol. 32, no. 5, pp. 1017–1028, Sep 1994.
- [25] J.-S. Lee, M. R. Grunes, and E. Pottier, "Quantitative comparison of classification capability: fully polarimetric versus dual and single-polarization SAR," *IEEE Transactions on Geoscience and Remote Sensing*, vol. 39, no. 11, pp. 2343–2351, nov 2001.
- [26] M. Hagedorn, P. J. Smith, P. J. Bones, R. P. Millane, and D. Pairman, "A trivariate chi-squared distribution derived from the complex Wishart distribution," *Journal of Multivariate Analysis*, vol. 97, no. 3, pp. 655–674, Mar. 2006.
- [27] S. Theodoridis and K. Koutroumbas, *Pattern Recognition*, Academic Press, 4 edition, 2008.
- [28] B. Picinbono, "Second-order complex random vectors and normal distributions," *IEEE Transactions on Signal Processing*, vol. 44, no. 10, pp. 2637–2640, oct 1996.
- [29] M. A. Sousa Júnior, L. V. Dutra, and C. C. Freitas, "Segmentação de imagens JERS e TM/Landsat usando o segmentador incremental multi-níveis SegSAR," in *Proceedings...*, J. C. N. Epiphany and L. M. G. Fonseca, Eds., São José dos Campos, 2005, Simpósio Brasileiro de Sensoriamento Remoto, 12 (SBSR), pp. 4493–4500, INPE.
- [30] R. G. Congalton and K. Green, *Assessing the Accuracy of Remotely Sensed Data: Principles and Practices*, CRC Press, Boca Raton, Florida USA, 2nd edition, 2009.

- [31] L. Bombrun, Y. Berthoumieu, N.-E. Lasmar, and G. Verdoolaege, "Multivariate texture retrieval using the geodesic distance between elliptically distributed random variables," in *Proceedings 18th IEEE International Conference on Image Processing*, 2011.
- [32] G. Verdoolaege and P. Saeunders, "Geodesics on the manifold of multivariate generalized Gaussian distributions with an application to multicomponent texture discrimination," *International Journal of Computer Vision*, vol. 95, pp. 265–286, 2011.
- [33] M. Berkane and K. Oden, "Geodesic estimation in elliptical distributions," *Journal of Multivariate Analysis*, vol. 63, pp. 35–46, 1997.
- [34] K. L. P. Vasconcellos, A. C. Frery, and L. B. Silva, "Improving estimation in speckled imagery," *Computational Statistics*, vol. 20, no. 3, pp. 503–519, 2005.
- [35] M. Silva, F. Cribari-Neto, and A. C. Frery, "Improved likelihood inference for the roughness parameter of the GA0 distribution," *Environmetrics*, vol. 19, no. 4, pp. 347–368, 2008.
- [36] F. Cribari-Neto, A. C. Frery, and M. F. Silva, "Improved estimation of clutter properties in speckled imagery," *Computational Statistics and Data Analysis*, vol. 40, no. 4, pp. 801–824, 2002.
- [37] H. Allende, A. C. Frery, J. Galbiati, and L. Pizarro, "M-estimators with asymmetric influence functions: the GA0 distribution case," *Journal of Statistical Computation and Simulation*, vol. 76, no. 11, pp. 941–956, 2006.
- [38] O. H. Bustos, M. M. Lucini, and A. C. Frery, "M-estimators of roughness and scale for GA0-modelled SAR imagery," *EURASIP Journal on Applied Signal Processing*, vol. 2002, no. 1, pp. 105–114, 2002.
- [39] A. C. Frery, J. Jacobo-Berlles, J. Gambini, and M. Mejail, "Polarimetric SAR image segmentation with B-Splines and a new statistical model," *Multidimensional Systems and Signal Processing*, vol. 21, pp. 319–342, 2010.



Wagner B. Silva received the B.Sc. and M.Sc. degrees in cartographic engineering from the Instituto Militar de Engenharia, Rio de Janeiro, Brazil, in 1999 and 2005, respectively. He is currently working toward the Ph.D. degree in Remote Sensing in the Instituto Nacional de Pesquisas Espaciais (INPE), São José dos Campos, Brazil. His research interests include stochastic models and SAR image processing.



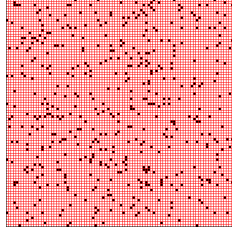
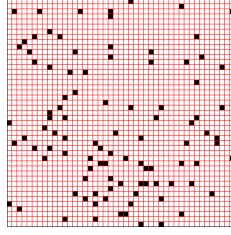
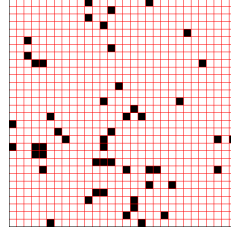
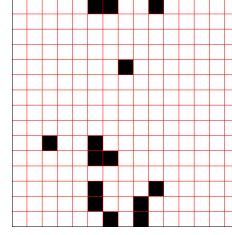
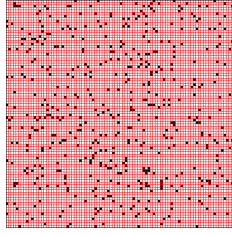
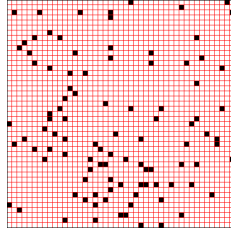
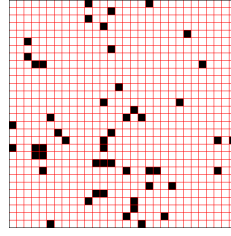
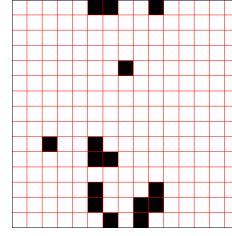
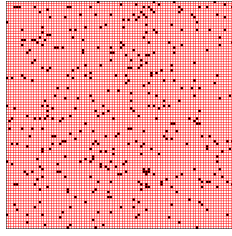
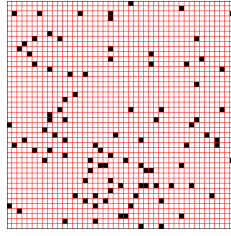
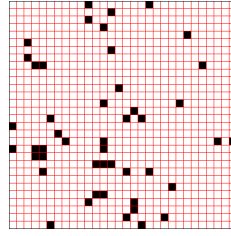
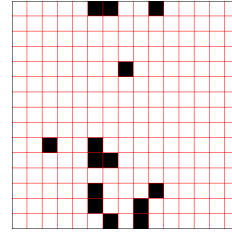
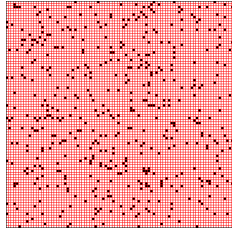
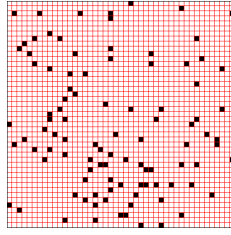
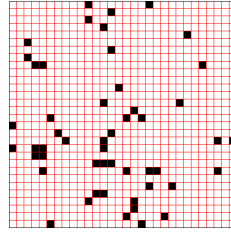
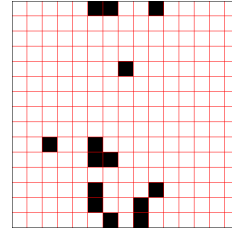
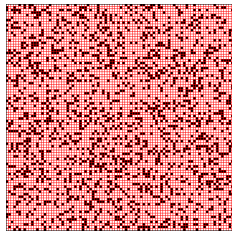
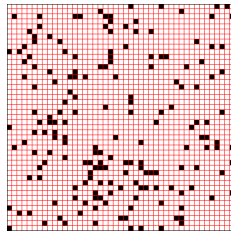
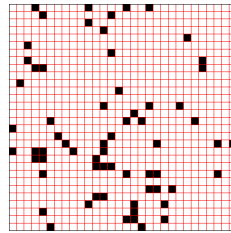
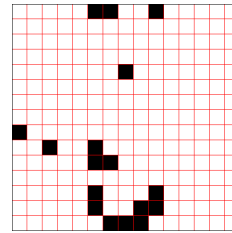
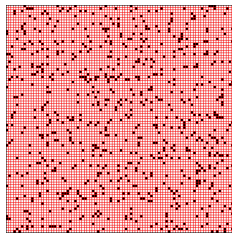
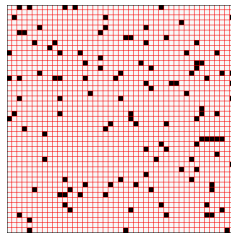
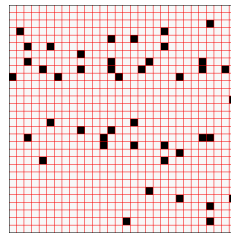
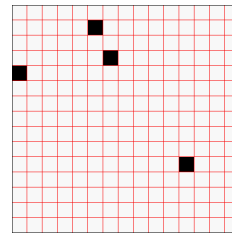
Corina C. Freitas received the B.S. degree in mathematics from the Pontifícia Universidade Católica de São Paulo in 1974, the M.Sc. degree in statistics from the Massachusetts Institute of Technology, Cambridge, in 1980, and the Ph.D. degree in statistics from the University of Sheffield, UK, in 1992. She is currently a Researcher at the Instituto Nacional de Pesquisas Espaciais (INPE), São José dos Campos, Brazil. Her research interests include statistical analysis of SAR images and SAR image processing.



Sidnei J. S. Sant'Anna received the B.S. degree in electrical and electronic engineer from the Universidade Federal do Rio de Janeiro in 1993, the M.Sc. degree in Remote Sensing from the Instituto Nacional de Pesquisas Espaciais (INPE), São José dos Campos, Brazil in 1995 and the Ph.D. degree in Eletronic Engineering and Computing from the Instituto Tecnológico de Aeronáutica (ITA), São José dos Campos, Brazil, in 2009. He is currently a researcher at INPE, and his interests are image analysis and processing techniques for remote sensing (SAR image filtering, statistical methods, robustness, etc.).



Alejandro C. Frery (S'92–M'95) received the B.S. degree in electronic and electrical engineering from the Universidad de Mendoza, Mendoza, Argentina, the M.Sc. degree in applied mathematics (statistics) from the Instituto de Matemática Pura e Aplicada, Rio de Janeiro, Brazil, and the Ph.D. degree in applied computing from the Instituto Nacional de Pesquisas Espaciais, São José dos Campos, Brazil. He is currently with the Instituto de Computação, Universidade Federal de Alagoas, Maceió, Brazil. His research interests are statistical computing and stochastic modeling.

(a) Bhattacharyya 5×5 (b) Bhattacharyya 10×10 (c) Bhattacharyya 15×15 (d) Bhattacharyya 30×30 (e) Kullback-Leibler 5×5 (f) Kullback-Leibler 10×10 (g) Kullback-Leibler 15×15 (h) Kullback-Leibler 30×30 (i) Hellinger 5×5 (j) Hellinger 10×10 (k) Hellinger 15×15 (l) Hellinger 30×30 (m) Rényi of order β 5×5 (n) Rényi of order β 10×10 (o) Rényi of order β 15×15 (p) Rényi of order β 30×30 (q) χ^2 5×5 (r) χ^2 10×10 (s) χ^2 15×15 (t) χ^2 30×30 (u) Bhatt. Gaussian 5×5 (v) Bhatt. Gaussian 10×10 (w) Bhatt. Gaussian 15×15 (x) Bhatt. Gaussian 30×30

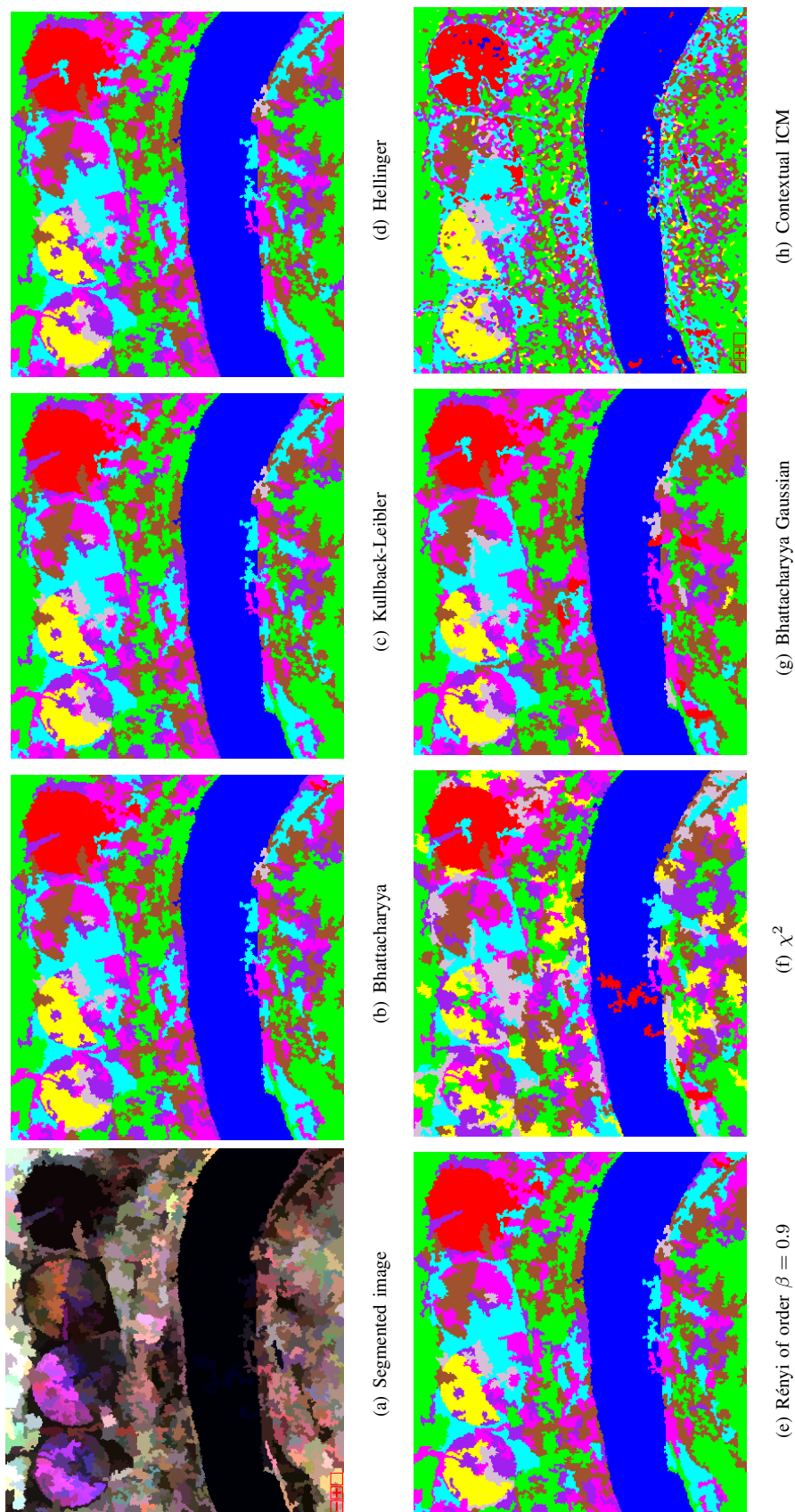


Fig. 5. SIR-C image segmentation and classification results.

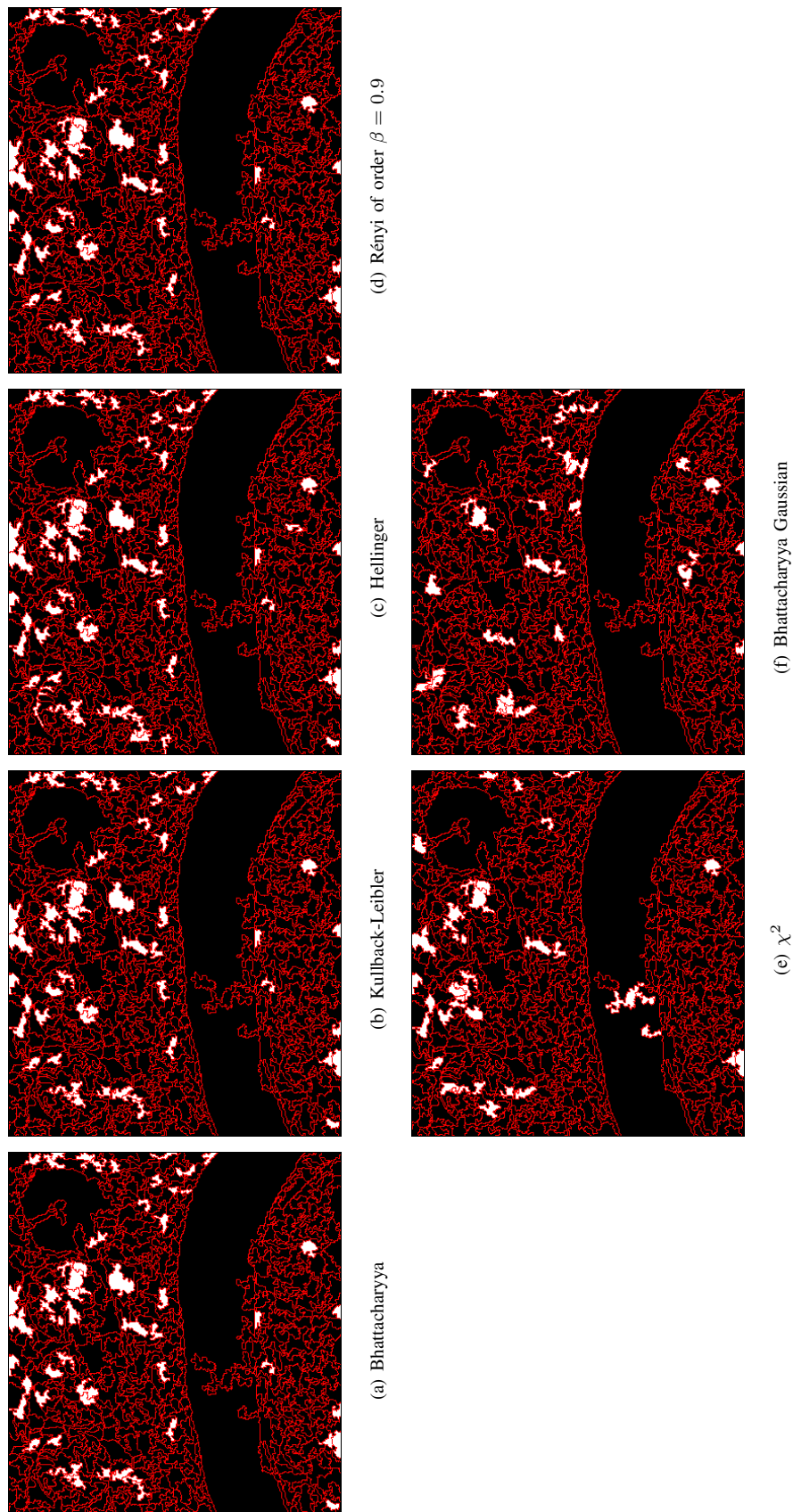


Fig. 6. P -value binary maps for SIR-C image classifications - segments in white have null hypothesis accepted ($p \geq 0.05$.)

$$\Sigma_{\text{river}} = \begin{bmatrix} 2.98 \cdot 10^{-3} & 5.31 \cdot 10^{-6} + j8.11 \cdot 10^{-5} & 3.47 \cdot 10^{-3} + j3.42 \cdot 10^{-4} \\ & 3.40 \cdot 10^{-4} & 4.47 \cdot 10^{-6} + j1.39 \cdot 10^{-4} \\ & & 1.19 \cdot 10^{-2} \end{bmatrix} \quad (14)$$

$$\Sigma_{\text{caatinga}} = \begin{bmatrix} 1.11 \cdot 10^{-1} & -3.10 \cdot 10^{-3} - j1.58 \cdot 10^{-3} & 1.98 \cdot 10^{-2} + j1.65 \cdot 10^{-3} \\ & 3.40 \cdot 10^{-2} & -1.41 \cdot 10^{-3} + j1.87 \cdot 10^{-3} \\ & & 9.47 \cdot 10^{-2} \end{bmatrix} \quad (15)$$

$$\Sigma_{\text{prep soil}} = \begin{bmatrix} 1.05 \cdot 10^{-2} & -5.39 \cdot 10^{-6} - j2.37 \cdot 10^{-4} & 7.53 \cdot 10^{-3} + j1.75 \cdot 10^{-3} \\ & 8.46 \cdot 10^{-4} & -3.38 \cdot 10^{-5} + j1.32 \cdot 10^{-4} \\ & & 1.14 \cdot 10^{-2} \end{bmatrix} \quad (16)$$

$$\Sigma_{\text{soybean 1}} = \begin{bmatrix} 3.40 \cdot 10^{-2} & -1.79 \cdot 10^{-3} - j1.86 \cdot 10^{-3} & -3.6 \cdot 10^{-4} - j7.58 \cdot 10^{-3} \\ & 5.16 \cdot 10^{-3} & 4.38 \cdot 10^{-4} + j4.28 \cdot 10^{-4} \\ & & 5.38 \cdot 10^{-2} \end{bmatrix} \quad (17)$$

$$\Sigma_{\text{soybean 2}} = \begin{bmatrix} 4.31 \cdot 10^{-2} & -1.76 \cdot 10^{-3} - j1.32 \cdot 10^{-3} & -1.78 \cdot 10^{-4} - j1.73 \cdot 10^{-3} \\ & 9.26 \cdot 10^{-3} & 6.55 \cdot 10^{-4} + j1.27 \cdot 10^{-3} \\ & & 4.35 \cdot 10^{-2} \end{bmatrix} \quad (18)$$

$$\Sigma_{\text{soybean 3}} = \begin{bmatrix} 7.53 \cdot 10^{-2} & -4.25 \cdot 10^{-3} - j7.66 \cdot 10^{-3} & 5.87 \cdot 10^{-4} - j1.36 \cdot 10^{-3} \\ & 1.47 \cdot 10^{-2} & -2.18 \cdot 10^{-4} + j1.21 \cdot 10^{-3} \\ & & 3.70 \cdot 10^{-2} \end{bmatrix} \quad (19)$$

$$\Sigma_{\text{tillage}} = \begin{bmatrix} 3.53 \cdot 10^{-2} & 1.20 \cdot 10^{-3} + j1.02 \cdot 10^{-4} & 1.64 \cdot 10^{-2} - j2.65 \cdot 10^{-3} \\ & 3.05 \cdot 10^{-3} & 4.48 \cdot 10^{-4} + j1.88 \cdot 10^{-4} \\ & & 3.29 \cdot 10^{-2} \end{bmatrix} \quad (20)$$

$$\Sigma_{\text{corn 1}} = \begin{bmatrix} 1.15 \cdot 10^{-1} & -3.95 \cdot 10^{-3} - j3.57 \cdot 10^{-3} & 9.13 \cdot 10^{-3} - j4.86 \cdot 10^{-3} \\ & 1.33 \cdot 10^{-2} & 3.34 \cdot 10^{-3} + j2.83 \cdot 10^{-3} \\ & & 1.47 \cdot 10^{-1} \end{bmatrix} \quad (21)$$

$$\Sigma_{\text{corn 2}} = \begin{bmatrix} 4.19 \cdot 10^{-2} & 1.08 \cdot 10^{-3} - j1.01 \cdot 10^{-3} & 9.24 \cdot 10^{-3} - j3.68 \cdot 10^{-3} \\ & 1.02 \cdot 10^{-2} & 2.43 \cdot 10^{-4} + j3.31 \cdot 10^{-4} \\ & & 5.71 \cdot 10^{-2} \end{bmatrix} \quad (22)$$
